Structural Evolution of MOF-Derived RuCo, A General Catalyst for the Guerbet Reaction

ACS APPLIED MATERIALS & INTERFACES

www.acsami.org

Forum Article

Structural Evolution of MOF-Derived RuCo, A General Catalyst for the Guerbet Reaction

Constanze N. Neumann, Michael T. Payne, Steven J. Rozeveld, Zhenwei Wu, Guanghui Zhang, Robert J. Comito, Jeffrey T. Miller, and Mircea Dincă*

Cite This: https://doi.org/10.1021/acsami.1c09873

Read Online

ACCESS | Metrics & More | Article Recommendations | Supporting Information

ABSTRACT: Guerbet alcohols, a class of β-branched terminal alcohols, find widespread application because of their low melting points and excellent fluidity. Because of the limitations in the activity and selectivity of existing Guerbet catalysts, Guerbet alcohols are not currently produced via the Guerbet reaction but via hydroformylation of oil-derived alkenes followed by aldol condensation. In pursuit of a one-step synthesis of Guerbet alcohols from simple linear alcohol precursors, we show that MOF-derived RuCo alloys achieve over a million turnovers in the Guerbet reaction of 1-propanol, 1-butanol, and 1-pentanol. The active catalyst is formed in situ from ruthenium-impregnated metal−organic framework MFU-1. XPS and XAS studies indicate that the precatalyst is composed of Ru precursor trapped inside the MOF pores with no change in the oxidation state or coordination environment of Ru upon MOF incorporation. The significantly higher reactivity of Ru-impregnated MOF versus a physical mixture of Ru precursor and MOF suggests that the MOF plays an important role in templating the formation of the active catalyst and/or its stabilization. XPS reveals partial reduction of both ruthenium and MOF-derived cobalt under the Guerbet reaction conditions, and TEM/EDX imaging shows that Ru is decorated on the edges of dense nanoparticles, as well as thin nanoplates of CoO_x. The use of ethanol rather than higher alcohols as a substrate results in lower turnover frequencies, and RuCo recovered from ethanol upgrading lacks nanostructures with plate-like morphology and does not exhibit Ru-enrichment on the surface and edge sites. Notably, ^{1}H and ^{31}P NMR studies show that through use of K_3PO_4 as a base promoter in the RuCo-catalyzed alcohol upgrading, the formation of carboxylate salts, a common side product in the Guerbet reaction, was effectively eliminated.

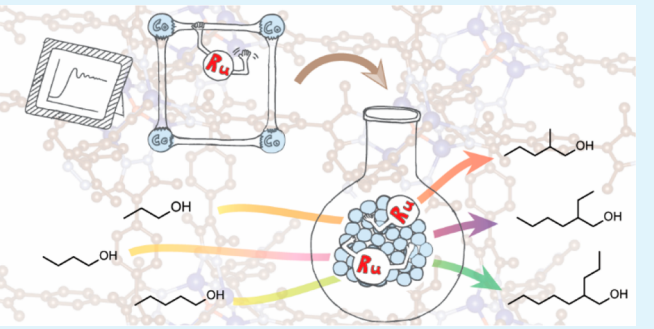

KEYWORDS: *Guerbet reaction, RuCo, 2-ethylhexanol, MOF-derived catalyst, alcohol upgrading*

INTRODUCTION

To enable full incorporation of fermentation and biomass-derived renewable feedstock into the production of fuels and chemicals, new catalysts are required to convert biobased oxygenates into commodity chemicals.[1] Unlike aliphatic petrochemical precursors, which are apolar and devoid of reactive functional groups, renewable feedstock is generally more highly oxygenated than the targeted products. Efficient use of renewable feedstock will thus rely on the development of highly active catalysts for transformations that reduce the oxygen content, extend carbon chain lengths, and enable selective transformation of polar, functionalized substrates with high selectivity.[2] Condensation reactions like the Guerbet reaction are of particular utility in the conversion of small oxygenates, such as short-chain alcohols, into useful fuels and commodity chemicals.[3] The high energy density, low water-miscibility and low corrosivity of 1-butanol render it promising as a second generation biofuel, which has inspired many recent reports on catalysts for the sustainable production of 1-butanol.[4−6] Original access to 1-butanol was provided by the acetone-butanol-ethanol (ABE) process whereby the *microorganism Clostridium acetobutylicum* converts sugar into valuable feedstocks.[6] The biochemical route was supplanted by cost-efficient chemical synthesis of 1-butanol from petrochemical-derived propene via hydroformylation, but the need for sustainable liquid transportation fuels has renewed interest in biochemical approaches to the synthesis of 1-butanol.[7] New microbial strains, as well as innovation in the fermentation setup, have significantly improved the productivity of microbial 1-butanol synthesis, but isolation of low concentrations of the alcohol from aqueous solution is both costly and energy intensive.[5,6,8,9] Heterogeneous catalysts for ethanol upgrading generally require reaction temperatures of

Special Issue: Emerging Materials for Catalysis and Energy Applications

Received: May 28, 2021
Accepted: August 5, 2021

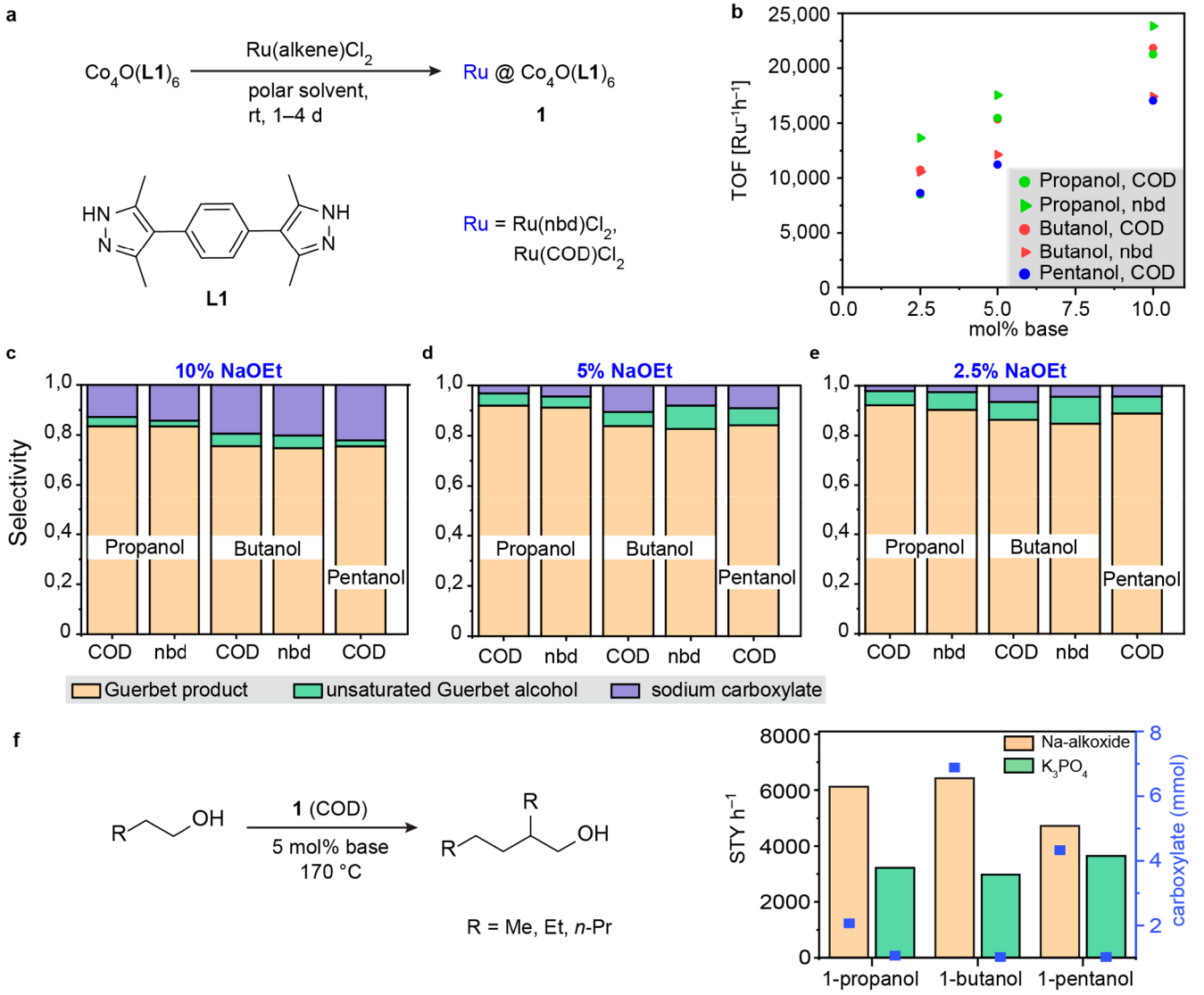

Figure 1. (a) Preparation of catalyst **1**. Activity (b) and selectivity for desired Guerbet product (c), sodium carboxylate derived from starting alcohol (d), and unsaturated derivatives of the desired Guerbet product (e) for the Guerbet reaction of 1-propanol, 1-butanol, and 1-pentanol catalyzed by **1** ([Ru] = 0.0027 mmol) using varying amounts of sodium alkoxide promoter. For 1-propanol and 1-butanol, results using **1** derived from either $Ru(nbd)Cl_2$ or $Ru(COD)Cl_2$ are shown. (**f**) Comparative site time yields per hour for formation of desired Guerbet product using either sodium alkoxide or K_3PO_4 as a base promoter. See Figures S1–S6 and Tables S1–6 for detailed results and reaction conditions.

250 °C or more to achieve suitable reaction rates, but the reduced activity is offset by the low price and recyclability of the catalyst in many of these systems.[10−25] While the lack of base promoter prevents the formation of sodium acetate, other side products, such as higher alcohols, CO, alkenes, or ethyl acetate, are commonly formed alongside the desired 1-butanol product. Recently developed homogeneous ruthenium, iridium, and manganese catalysts for the Guerbet reaction of fermentation-derived ethanol can achieve high turnover numbers and high selectivity among liquid products for the formation of 1-butanol at moderate conversions.[26−34] Use of base promoters, such as NaOEt, commonly result in the formation of sodium acetate alongside the desired 1-butanol product, but high catalyst activity can be achieved at temperatures at or below 160 °C.

Transition metals are readily reduced to the metallic state by H_2 released during the Guerbet reaction in the basic alcohol reaction medium commonly employed, rendering it difficult to sufficiently stabilize a homogeneous catalyst for long-term use.[35−37] Furthermore, the metallic deposit has, in some cases, been shown to be the main contributor to catalytic activity.[35] MOFs, being both porous and densely functionalized, can function as a suitable support for both oxidized and reduced versions of the catalytically active metal. In addition to acting as a catalyst support, the metals contained in the MOF secondary building unit (SBU) can take an active part in catalytic conversion. Indeed, we have found that the positive cooperative effect of nickel on both the efficiency and selectivity of ruthenium-catalyzed ethanol upgrading was strongly enhanced when a Ni-based MOF acted as catalyst support and source of nickel.[38] Supported RuNi alloy nanoparticles, formed in situ, could achieve turnover numbers (TON) up to 750 000 Ru^{-1} at 170 °C for ethanol upgrading while showing negligible activity toward the 1-butanol product. Subsequent development of a catalyst for 1-butanol upgrading through simple replacement of the MOF precursor validated

https://doi.org/10.1021/acsami.1c09873
ACS Appl. Mater. Interfaces XXXX, XXX, XXX−XXX

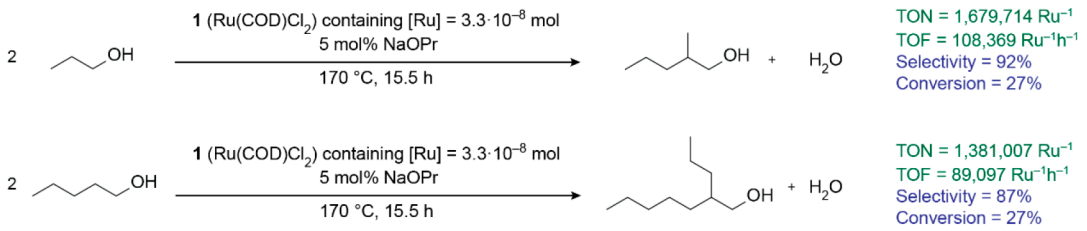

Figure 2. Optimized conditions for 1-propanol and 1-pentanol upgrading catalyzed by **1** conducted in a stainless steel pressure reactor at 170 °C (see Tables S7−S9 for details).

that in situ formation of catalytically active Ru-alloy nanostructures from Ru-impregnated MOF precursors constitutes a tunable design approach for Guerbet catalysts. MOF-derived RuCo nanoparticles catalyze upgrading of 1-butanol to the high-volume chemical 2-ethylhexanol with TON > 10^6 Ru^{-1} at 170 °C.[39]

Our previous studies were aimed at the development of the optimized MOF-derived catalytic systems for the synthesis of isolated alcohol substrates, which are currently produced on large scales in a nonrenewable fashion. However, many Guerbet alcohols, with feature distinctive β-branching that engenders high liquidity and oxidative stability, find application in lubrication, paper processing and personal care products.[3,40,41] Yet, reports, especially of a recent nature, on self-condensation of short-chain alcohols other than ethanol to high-volume Guerbet alcohols have been scarce.[35,36,42−51] Here, we show that MOF-derived alloys can function as *general* Guerbet catalysts with high catalytic activity for a suite of alcohol substrates, such as 1-propanol, 1-butanol and 1-pentanol. We have previously shown the superior catalytic performance of MOF-derived RuCo, formed in situ from bench stable precursors, over RuCo nanoparticles supported on a variety of traditional supports.[39] In an effort to understand why Ru-impregnated MFU-1[52,53] serves as a superior precursor of supported RuCo nanoparticles we investigate the changes in ruthenium coordination environment and oxidation state upon incorporation into the MOF support, as well as the importance of the ligands present on the impregnation precursor. To eliminate solvent waste and maximize the space-time yield, all Guerbet reactions with MOF-derived catalysts are conducted neat, so that the reaction substrate simultaneously functions as the reaction solvent for the upgrading reaction as well as the in situ reductant for the formation of the catalytically active RuCo species. Since efficient alcohol upgrading reactions with the same catalyst can be performed using 1-propanol, 1-butanol, and 1-pentanol, and to a lesser degree, ethanol, we were able to examine the effect of the substrate/solvent on the composition and morphology of RuCo nanostructures formed.

EXTENSION OF MOF-DERIVED RU ALLOY-CATALYSIS TO OTHER GUERBET SUBSTRATES

Encouraged by the dramatic increase in catalytic activity of ruthenium salts in the Guerbet reaction of 1-butanol when supported on MFU-1 ($Ru@Co_4O(\mathbf{L1})_6$, **1**),[39] we set out to investigate if the Guerbet reaction of 1-propanol and 1-pentanol could similarly be catalyzed by **1** (Figures 1a and S1−S3). Notably, we found that 1-pentanol can be upgraded to 2-propylheptanol with almost equal efficiency and comparable selectivity to that observed for 1-butanol (Figure 1b−e). The effect of the concentration of the sodium alkoxide base promoter (sodium propoxide for 1-propanol upgrading, sodium butoxide for 1-butanol upgrading, and sodium pentoxide for 1-pentanol upgrading) on both the catalyst activity and the selectivity with which the desired product is formed shows a remarkably similar trend to that observed for 1-butanol. In addition to the expected carboxylate product commonly formed in base-promoted Guerbet reactions via a competing Cannizzaro or Tishchenko reaction,[3,27,30−33,48,54,55] products of incomplete reduction can be formed alongside the desired Guerbet alcohol (see Figures 1e and S4). Notably, higher catalytic activity for **1** was observed in the upgrading of 1-propanol compared to that previously reported for 1-butanol,[39] and the selectivity for the formation of the desired Guerbet product 2-methylpentanol was likewise increased, particularly in the presence of high loadings of base promoter. The identity of the ruthenium precursor ($Ru(nbd)Cl_2$, nbd = norbornadiene or $Ru(COD)Cl_2$, COD = cyclooctadiene) used to generate **1** has a small, but noticeable effect on the reaction efficiency and selectivity for all alcohols tested. The sodium alkoxide solutions used throughout this work were prepared by dissolving sodium in the corresponding alcohol, because substantial contamination of commercial batches of sodium alkoxide with sodium carboxylates and sodium carbonate has been reported.[56] While we did not observe any decomposition products of sodium alkoxide batches up to 10 months after preparation by ^{1}H NMR or ^{13}C NMR analysis (Figures S2 and S3), potential reproducibility issues arising from degradation of alkoxide batches further motivated the exploration of alternative bases.

Gratifyingly, alcohol upgrading with **1** also proceeded effectively when the sodium alkoxide cocatalyst was replaced by K_3PO_4 (Figure 1f), and essentially no sodium carboxylate side product was formed when the weaker base was employed (Figure S5). Because of the different side product profile, we analyzed the effect of the base promoter on the site time yield (STY) for the formation of the desired Guerbet alcohol rather than on the TOF, which is derived from the conversion of the starting alcohol and thus takes into account all products formed in the reaction (Figure 1f). Notably, the change in base affected the relative activity of the catalyst toward the different alcohol substrates: While 1-pentanol displayed the lowest activity in the series with **1**/sodium alkoxide, the reverse was observed with **1**/K_3PO_4 (Figure 1f). When soluble alkoxide bases are used, the amount of sodium carboxylate side product can be determined by simple precipitation of the salts from the reaction mixture with acetone and gravimetric determination of amount of solid removed by filtration. Analysis by PXRD of the recovered solids from alcohol upgrading reactions catalyzed by **1**/K_3PO_4 did not reveal any diffraction peaks indicative of carboxylate formation (Figure S7). Since any amorphous solids formed during the reaction would not appear in the diffraction pattern, we further analyzed the recovered

https://doi.org/10.1021/acsami.1c09873
ACS Appl. Mater. Interfaces XXXX, XXX, XXX−XXX

Table 1. Ethanol Upgrading[a]

run	variable	Ru source	[Ru][b]	base[c] (%)	TON	TOF	conv[d]	selectivity[e]
1	Ru source	**$Ru(nbd)Cl_2$**	4.32×10^{-7}	5	55 590	**3088**	0.07	**0.83**
2		**$Ru(COD)Cl_2$**	4.32×10^{-7}	5	63 196	**3511**	0.08	**0.80**
3	base concentration	$Ru(nbd)Cl_2$	2.07×10^{-7}	**18**[f]	216 151	13 301	0.13	**0.54**
4		$Ru(nbd)Cl_2$	4.32×10^{-7}	**10**	86 051	4988	0.11	**0.73**
5		$Ru(nbd)Cl_2$	4.32×10^{-7}	**5**	55 590	3088	0.07	**0.83**
6	catalyst loading	$Ru(COD)Cl_2$	**1.29×10^{-6}**	5	22 452	**554**	0.09	0.76

[a]Conditions: 20.0 mL NaOEt in ethanol, stainless steel Parr reactor, 170 °C. [b]Amount of ruthenium [moles]. [c]Concentration of NaOEt. [d]Conversion of ethanol. [e]Selectivity for butanol formation. For control reactions with unsupported ruthenium and cobalt compounds, see Table S2. [f]18 mol % base concentration corresponds to 21 wt %.

solid by ^1H and ^{31}P NMR in D_2O using tetraethylphosphonium tetrafluoroborate (TEP BF_4^-) as an internal standard. We found that under conditions where 196 mg of sodium propanoate where formed using NaOPr as a base additive, less than 2 mg of potassium propanoate were formed using K_3PO_4 as the base (Figure S8). Similarly, with **1**/K_3PO_4, <1 mg of carboxylate was formed in butanol upgrading (760 mg with **1**/NaOBu), and <2 mg in 1-pentanol upgrading (537 mg with **1**/NaOPent, Figures 1f, S9, and S10).

The catalyst loading could also be reduced from [Ru] = 2.7×10^{-6} mol to [Ru] = 3.3×10^{-8} mol without a substantial decrease in the conversion achieved after 15 h, and under the optimized reaction conditions, TON = 1 679 714 Ru^{-1} (TOF = 108 369 Ru^{-1} h^{-1}) was observed for the upgrading of 1-propanol, and TON = 1 381 007 Ru^{-1} (TOF = 89 097 Ru^{-1} h^{-1}) for the upgrading of 1-pentanol (Figure 2). RuCo nanoparticle catalysts formed in situ from a cobalt-based MOF impregnated with ruthenium can thus be employed for the efficient synthesis of a variety of branched Guerbet alcohols. This contrasts with our earlier developed MOF-derived RuNi catalyst system, which can deliver exquisite selectivity for the *linear* Guerbet product 1-butanol by virtue of its negligible activity for the further conversion of 1-butanol to 2-ethylhexanol.[38]

While reduced product selectivity would be expected with **1** in the upgrading of ethanol to 1-butanol because of the established high activity of **1** for the Guerbet reaction of 1-butanol to 2-ethylhexanol, we were nonetheless interested to see if **1** showed comparable activity for ethanol upgrading to that observed with terminal C_2–C_5 alcohols. We found that while ethanol upgrading with **1** could be achieved, the turnover frequency (TOF) measured with ethanol as the reaction substrate was substantially lower than was observed with 1-propanol, 1-butanol, or 1-pentanol. Furthermore, despite our best efforts, we were unable to achieve ethanol conversions exceeding 10% under reaction conditions that furnish 1-butanol with >73% selectivity (Table 1), even if the reaction time was prolonged to 65 h (Table S10, entry 9). An increase in the catalyst loading similarly did not result in an increase of the conversion beyond 9% (Table 1, entry 6), but merely led to a decrease in the TOF. A high turnover frequency (13 301 Ru^{-1} h^{-1}) and a conversion of 13% could only be achieved by employing a low catalyst loading and increasing the base concentration to 18 mol % NaOEt (which corresponds to 21 wt % NaOEt).[38] At these concentrations of base promoter, however, the selectivity for 1-butanol was only 0.54, and furthermore, substantial leaching of catalytically active nanoparticles from the catalyst support was observed.

We performed a combination of hot filtration experiments, UV–vis, and transmission electron microscopy (TEM) analyses of filtered reaction mixtures to gain insight into the nature of Ru species leached from MOF-supported RuCo (Figures 3 and S11–S13). Ethanol upgrading experiments in

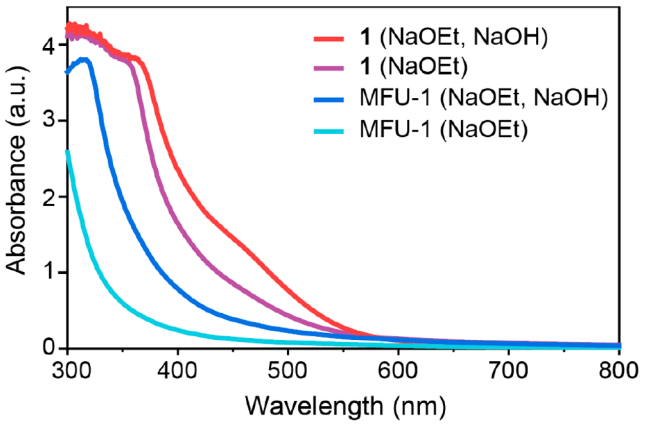

Figure 3. UV–vis spectrum of ethanol upgrading reaction mixture, including **1** (purple) or MFU-1 (turquoise) and 18 mol % NaOEt, filtered after 4 h at 170 °C. The additional presence of small quantities of water in the ethanol upgrading reaction led to more pronounced absorption for both **1** (red), or MFU-1 (blue).

the presence of 18 mol % NaOEt were carried out both with **1** and with the Ru-free support MFU-1 for 4 h at 170 °C and after cooling to 70 °C, the reaction mixture was filtered to remove particles >200 μm. During the Guerbet reaction, an equimolar amount of water is formed along with the upgrading product, so that both alkoxide and hydroxide are present under the reaction conditions, either of which could give rise to metal leaching. Since no Guerbet reaction and, hence, no NaOH formation is expected in the absence of Ru (see Figure 4c), the same experiment was also repeated with deliberate addition of water to the reaction mixture (see Table S11) to simulate reaction conditions after substantial conversion for experiments with both **1** and MFU-1. The filtrate of ethanol upgrading reaction mixtures conducted in the absence of ruthenium (pure MFU-1 support) shows featureless absorption in the visible region extending past 500 nm, which indicates the presence of metal nanoparticles (Figure 3).[57] The addition of 1.5 at% Ru (relative to the cobalt content of the support) however, led to a substantial increase in the absorption intensity in the visible region of the filtered reaction.[58] The substantial absorption in the visible range indicates that both Co (pure MFU-1) and either RuCo or a mixture of Ru and Co (Ru@MFU-1) were leached into the reaction mixture in the form of nanoparticles rather than as molecular species. A noticeable increase in absorption intensity

https://doi.org/10.1021/acsami.1c09873
ACS Appl. Mater. Interfaces XXXX, XXX, XXX–XXX

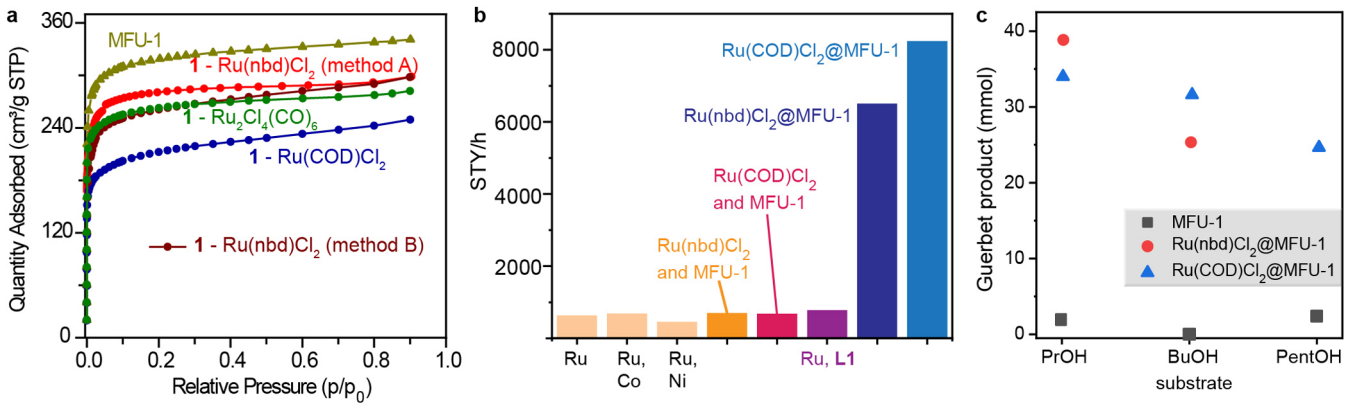

Figure 4. (a) Surface area of MFU-1 was reduced upon ruthenium incorporation. BET surface area of **1** ($Ru(nbd)Cl_2$, A), 1034 ± 6 $m^2 \cdot g^{-1}$; **1** ($Ru(nbd)Cl_2$, B), 881 ± 19 $m^2 \cdot g^{-1}$; **1** ($Ru(COD)Cl_2$), 804 ± 1 $m^2 \cdot g^{-1}$; **1** ($Ru_2Cl_4(CO)_6$), 1034 ± 1 m^2/g; MFU-1 used for ruthenium incorporation, 1268 ± 1 m^2/g (reported BET surface area for MFU-1 obtained by microwave synthesis (not shown in figure), 1485(50) m^2/g).[52,60] (b) STY for 2-ethylhexanol formation for 1-butanol upgrading reactions conducted at 170 °C (Table S12). (c) Comparison of alcohol upgrading catalyzed by MFU-1 in the presence and absence of ruthenium (Table S13).

was observed upon addition of water to the ethanol upgrading experiment (Figure 3 and Table S11), indicating that NaOEt, which was present at a >10-fold higher concentration than NaOH, has a less substantial effect on leaching than the hydroxide base (Figures S11−S13). Recent work by Han et al. detailed how the adverse effect of water on the selectivity and conversion of Ni−Co/HAP and TiO_2 catalyzed Guerbet reaction of 1-butanol can be mitigated by addition of 1,1-dibutoxybutane, which undergoes in situ hydrolysis to the alcohol substrate and corresponding aldehyde intermediate.[59] Leaching of RuCo nanoparticles caused by water-derived hydroxide is another deleterious outcome of the increase in the concentration of water with increased alcohol conversion and may thus be addressed by addition of an additive that removes water from the reaction mixture.

Hot filtration experiments confirmed that the metal nanoparticles leached into the reaction mixture were catalytically active. Substantial leaching of the catalytically active metal nanoparticles into a reaction mixture devoid of stabilizing ligands may account for the substantial activity but limited conversion observed with **1** in ethanol upgrading reactions. For higher alcohol substrates, substantial conversions are accessible with the same catalyst, but significantly lower amounts of base promoter. We had previously found that leaching of catalytically active RuCo from the MOF support was observed in butanol upgrading reactions promoted by 10 mol % NaOBu, whereas leaching was completely absent for reactions carried out in the presence of 5 mol % NaOBu.[39] Only substrates displaying the targeted level of activity in the presence of 5 mol % sodium alkoxide or K_3PO_4 are thus well suited for catalysis by **1**, because the metal−support interaction between RuCo and the MFU-1 appear to be insufficiently strong to completely retain the catalytically active nanoparticles in the presence of larger amounts of base. Furthermore, it suggests that RuNi is more tightly bound to the MOF support from which it is derived than RuCo, because the use of 18 mol % NaOEt base promoter did not result in substantial leaching in ethanol upgrading reactions.[38]

CHARACTERIZATION OF MOF-INCORPORATED RUTHENIUM PRECATALYSTS

To aid in further efforts to improve the performance of MOF-derived Ru-alloy catalysts, we examined the effect of pore incorporation on the coordination environment of ruthenium, and the changes in structure and chemical properties observed upon conversion to the presumed active species. Synthesis of **1** involves soaking of the preformed MOF in a suspension of a suitable ruthenium compound in a polar solvent, leading to ruthenium incorporation as detected by ICP-MS and a significant reduction in surface area (Figure 4a). Washing of ruthenium-incorporated MOFs with DMF, ethanol, methanol, acetone, or MeCN does not lead to a noticeable reduction in the ruthenium content, and the crystal structure of the MOF is retained upon ruthenium incorporation. Control experiments were carried out to determine whether the increased activity of $Ru(nbd)Cl_2$ or $Ru(COD)Cl_2$ when supported on MFU-1 was simply due to the presence of a source of Co^{II} or the nitrogenous ligand used as a linker in MFU-1 (Figure 4b, Table S12). While a small increase in activity was observed in the presence of **L1** or a cobalt (but not a nickel) salt, the catalytic activity in 1-butanol upgrading fell far short of that observed with **1**, which formed comparable amounts of 2-ethylhexanol after 14.5 h only when ruthenium loading was reduced 10-fold. Furthermore, we found that a physical mixture of MFU-1 and $Ru(nbd)Cl_2$ showed similar activity to pure $Ru(nbd)Cl_2$ rather than $Ru(nbd)Cl_2$@MFU-1 (**1**, Figure 4b). In the absence of ruthenium, on the other hand, none of the alcohol substrates tested afforded significant amounts of the Guerbet product in the presence of MFU-1 and 10 mol % sodium alkoxide promoter (Figure 4c, Table S13).

Given the high catalytic activity of **1**, care was taken to exclude catalytic contributions by impurities or cross-contamination between different experiments. Catalytically active rhodium nanoparticles have previously been immobilized on the surface of Teflon stir bars, and they were not dislodged by washing with organic solvents.[61] Between each alcohol upgrading experiment, the stir bar and stainless steel reactor was cleaned using a solution of KOH/^{i}PrOH, followed by soapy water, then water, and finally acetone. No change in catalytic results was observed when the reactor and stir bar were cleaned using concentrated sulfuric acid rather than

https://doi.org/10.1021/acsami.1c09873
ACS Appl. Mater. Interfaces XXXX, XXX, XXX−XXX

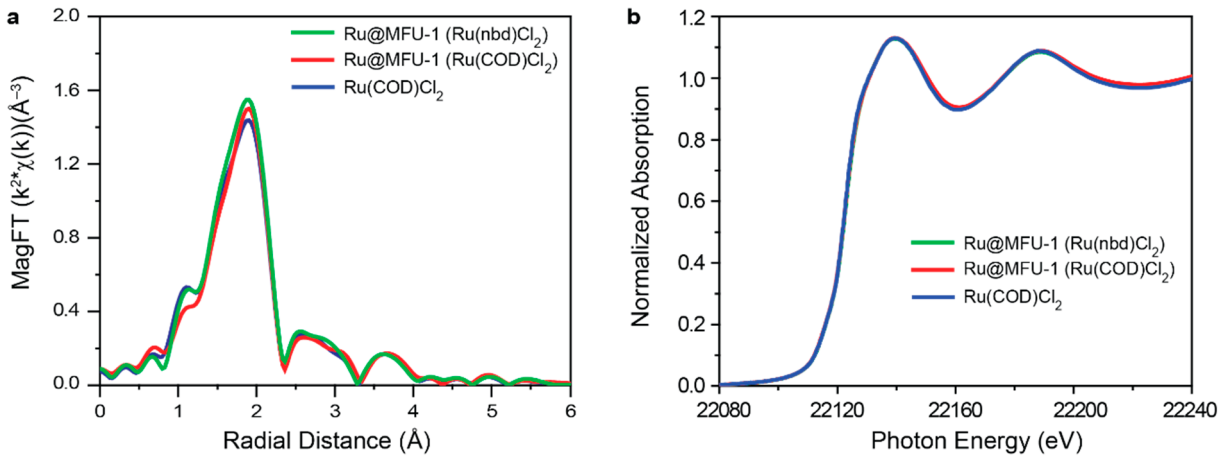

Figure 5. Comparison of (a) extended X-ray fine structure (EXAFS) and (b) X-ray absorption near edge spectra (XANES) of ruthenium alkene complexes incorporated into MFU-1 with $Ru(COD)Cl_2$.

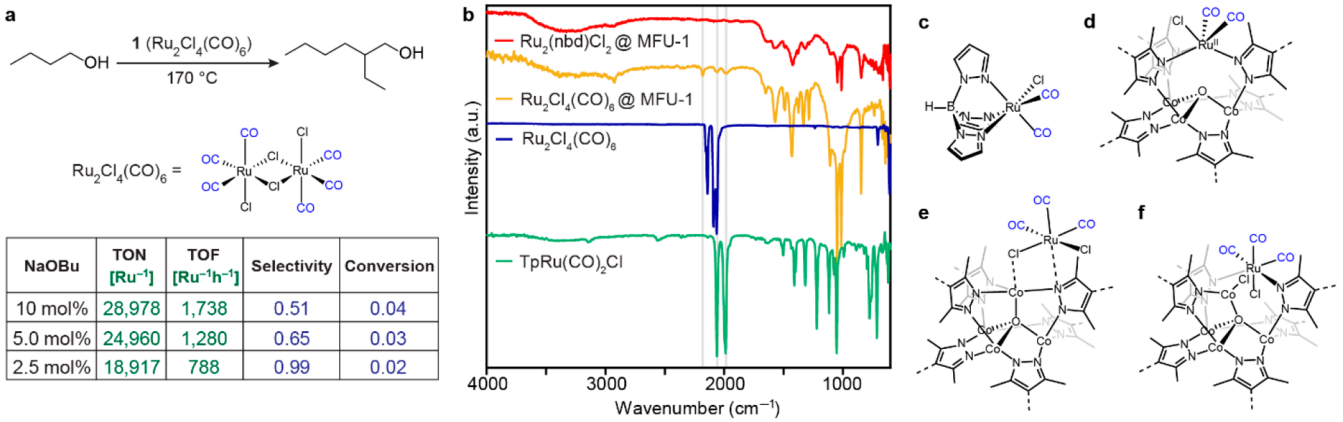

NaOBu	TON [Ru^{-1}]	TOF [$Ru^{-1}h^{-1}$]	Selectivity	Conversion
10 mol%	28,978	1,738	0.51	0.04
5.0 mol%	24,960	1,280	0.65	0.03
2.5 mol%	18,917	788	0.99	0.02

Figure 6. (a) Butanol upgrading catalyzed by **1** generated from $Ru_2Cl_4(CO)_6$ incorporated into MFU-1. (b) Comparison of IR spectra of $Ru_2Cl_4(CO)_6$@MFU-1 with $Ru(nbd)Cl_2$@MFU-1, $Ru_2Cl_4(CO)_6$, and $TpRu(CO)_2Cl$. (c) $TpRu(CO)_2Cl$ (d) SBU of MFU-1 having undergone Ru-cation exchange. (e) Cleavage of $Ru_2Cl_4(CO)_6$ by pyrazole linker. (f) Proposed structure for $Ru_2Cl_4(CO)_6$@MFU-1.

KOH/^{i}PrOH. Furthermore, no alteration in the catalytic results was observed either when a stir bar used for >50 reactions was replaced by an unused Teflon stir bar.[62] Catalytic reactions were carried out either directly inside a stainless steel Parr reactor or using a glass liner with no noticeable difference, so that the steel surface appears to neither aid nor hinder the progress of the reaction.[63] Most importantly, the control reactions with ruthenium-free support shown in Figure 4c were carried out after the vast majority of all catalytic alcohol upgrading reactions reported here, using the same equipment, chemicals and cleaning routine. The low levels of activity in propanol and pentanol upgrading and entire lack of activity in butanol upgrading of Ru-free MFU-1 furthermore indicate that cobalt does not itself display catalytic activity. The complementary substrate preference of RuNi and RuCo, however, suggests a substantial level of synergy between ruthenium and either cobalt or nickel in MOF-derived Ru-alloy catalysts.

To obtain insight into the coordination environment of the MOF-incorporated ruthenium compounds, we obtained X-ray absorption spectroscopy (XAS) data for **1** prepared using either $Ru(nbd)Cl_2$ and $Ru(COD)Cl_2$. A variety of standards that mimic various potential ligand exchange processes at the ruthenium center were analyzed (Figure S14). Despite the widely different reactivity observed with physical mixtures of MFU-1 and $Ru(nbd)Cl_2$ versus **1**, however, a striking resemblance in the XAS data of $Ru(COD)Cl_2$ and $Ru(COD)Cl_2$ incorporated into MFU-1 (**1**) was observed (Figure 5). XAS analysis thus confirmed that no cobalt to ruthenium cation exchange takes place at the SBU of MFU-1, and showed furthermore that no significant modification of the ruthenium coordination sphere occurs upon incorporation into the MOF.

EFFECT OF RUTHENIUM LIGAND

We then tested whether ruthenium precursors whose chemical and physical properties differ significantly from $Ru(nbd)Cl_2$ could be introduced into a MOF support in analogous fashion. We found that $Ru_2Cl_4(CO)_6$, which unlike $Ru(nbd)Cl_2$ readily dissolves in many organic solvents and features a significantly more electron-deficient ruthenium center, could successfully be incorporated into MFU-1 by soaking of MFU-1 in a solution of the ruthenium compound in EtOH or DMF (Figures 6a and S15–S18). Catalyst **1** derived from $Ru_2Cl_4(CO)_6$ as the ruthenium precursor instead of $Ru(COD)Cl_2$ or $Ru(nbd)Cl_2$ led to much lower activity for the upgrading of 1-butanol to 2-ethylhexanol (Figure 6a, Table S14). Furthermore, while no unsaturated Guerbet alcohol products could be detected, in the

https://doi.org/10.1021/acsami.1c09873
ACS Appl. Mater. Interfaces XXXX, XXX, XXX−XXX

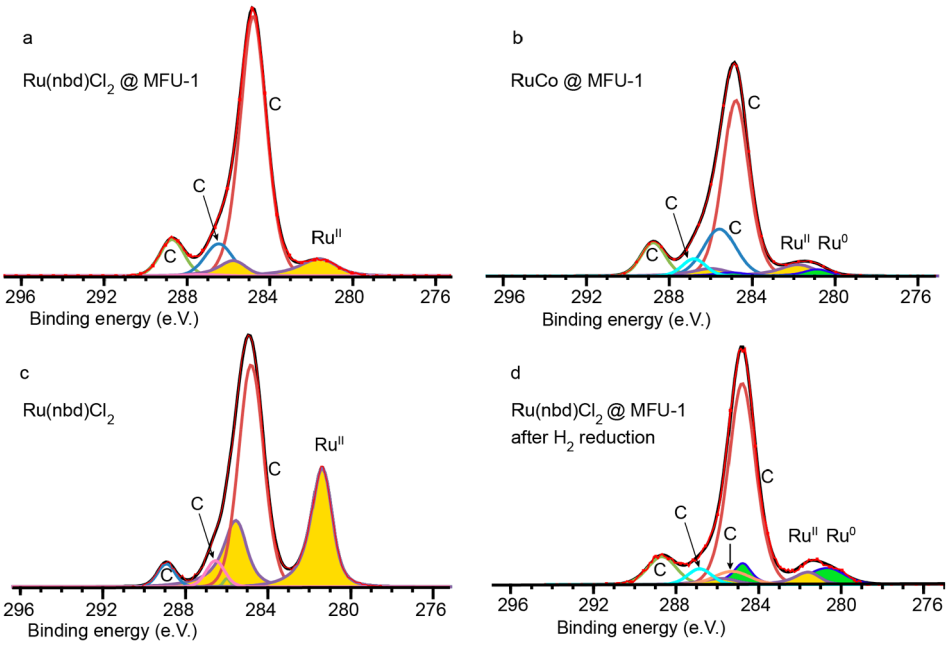

Figure 7. X-ray photoelectron spectroscopy analysis of the change of Ru oxidation state during in situ formation of the active catalyst. (a) **1** prior to being exposed to alcohol upgrading. (b) **1** recovered from alcohol upgrading. (c) $Ru(nbd)Cl_2$ used for the synthesis of **1**. (d) **1** after reduction by H_2.

presence of >2.5 mol % NaOBu base promoter, over 35% of 1-butanol consumed was converted into sodium butyrate rather than 2-ethylhexanol. We speculate that strong binding of CO ligands to the reduced metal active species formed in situ under the reaction conditions may account for the pronounced decrease in catalytic activity.

To test if structural differences between **1** derived from $Ru_2Cl_4(CO)_6$ and **1** synthesized using $Ru(nbd)Cl_2$ or $Ru(COD)Cl_2$ accompany the decreased activity, the ruthenium environment after incorporation into the MOF host was probed using infrared spectroscopy (IR). The CO ligand is a convenient IR handle since the carbonyl stretch of the ruthenium-bound CO ligand shifts upon modification of the coordination sphere of Ru. Carbonyl stretches at 2181, 2058, and 1985 cm^{-1} were observed for $Ru_2Cl_4(CO)_6$@MFU-1, which differ substantially from the carbonyl stretches of the ruthenium precursor $Ru_2Cl_4(CO)_6$ (2141, 2091, and 2064 cm^{-1}, Figure 6b).[64] Ruthenium−cobalt cation exchange in the MOF SBU was excluded due to the presence of a high frequency band, which is absent for ruthenium complexes featuring a tridentate nitrogen-donor ligand such as trispyrazoleborate (Tp) and only two carbonyl ligands (Figure 6b,c,d). A control experiment where $Ru_2Cl_4(CO)_6$ was exposed to ethanol (Figure S19), the solvent employed in the preparation of $Ru_2Cl_4(CO)_6$@MFU-1 (Figure 6a), shows that the CO stretching frequencies of $Ru_2Cl_4(CO)_6$ are not significantly altered by solvent exposure. In donor solvents, symmetrical cleavage of $Ru_2Cl_4(CO)_6$ to yield $RuCl_2(CO)_3(S)$ (S = solvent) is known to occur,[65] but in the case of ethanol, splitting of the dimer has been shown to be reversible upon solvent evaporation.[64] The remaining possible reaction sites are the linker or SBU of the MOF: displacement of the solvent ligand in $RuCl_2(CO)_3(S)$ by the pyrazole group of the MOF linker would yield a structure shown in Figure 6e, which may be further stabilized through the formation of a chloride bridge between Co and Ru.[66] Considering that the CO stretches reported for $Ru(CO)_3Cl_2$(pyridine) are 2136, 2075, and 2051 cm^{-1}, more than one strongly donating ligand must be present in the coordination sphere of $Ru_2Cl_4(CO)_6$@MFU-1.[67] A reasonable similarity between the carbonyl stretches observed for $Ru_2Cl_4(CO)_6$@MFU-1 and those reported for $Ru(CO)_3Cl$(glycinate) (2143.5, 2065.0, and 1989.0 cm^{-1})[68] and $Ru(CO)_3Cl(2,2'\text{-bipyridine})^+$ (2112.4, 2060.7, and 1993.3 cm^{-1}),[68] leads us to suggest the structure depicted in Figure 6f as the most reasonable assignment for $Ru_2Cl_4(CO)_6$@MFU-1. The complex shown in Figure 6f could be formed via transfer of chloride to the adjacent cobalt center upon displacement from ruthenium by the MOF linker, similar to chloride transfer to a second molecule of $Ru(CO)_3Cl(ROH)$ when this precursor reacts with a stoichiometric amount of bipyridine.[65] Prior examples of the coordination of two donor ligands to the ruthenium center with transfer of the chloride ligand to a different metal center provides support for our assignment of $Ru_2Cl_4(CO)_6$@MFU-1 as the structure shown in Figure 6f (Table S15, Figure S19). Because incorporation of a second-row transition metal into a MOF SBU is highly unusual, however, further studies are needed to conclusively establish the coordination geometry around ruthenium in $Ru_2Cl_4(CO)_6$@MFU-1.[69,70]

Formation of the Active Catalyst under the Reaction Conditions. The reaction conditions used for the Guerbet reaction are both basic and reductive, with H_2 being evolved in the dehydrogenation of the alcohol substrate during the first step of the Guerbet mechanism. Comparison of the Ru 3d X-ray photoelectron spectroscopy (XPS) signals of the pristine ruthenium-incorporated MFU-1 species (Figure 7a) and the ruthenium precursor $Ru(nbd)Cl_2$ (Figure 7c) shows no change in the binding energy of Ru 3d core electrons. This observation is in line with the XAS data for **1** (Figure 5), where no evidence of changes in the ruthenium coordination environment or oxidation state upon MOF incorporation could be found. Catalyst recovered from the alcohol upgrading reaction

https://doi.org/10.1021/acsami.1c09873
ACS Appl. Mater. Interfaces XXXX, XXX, XXX−XXX

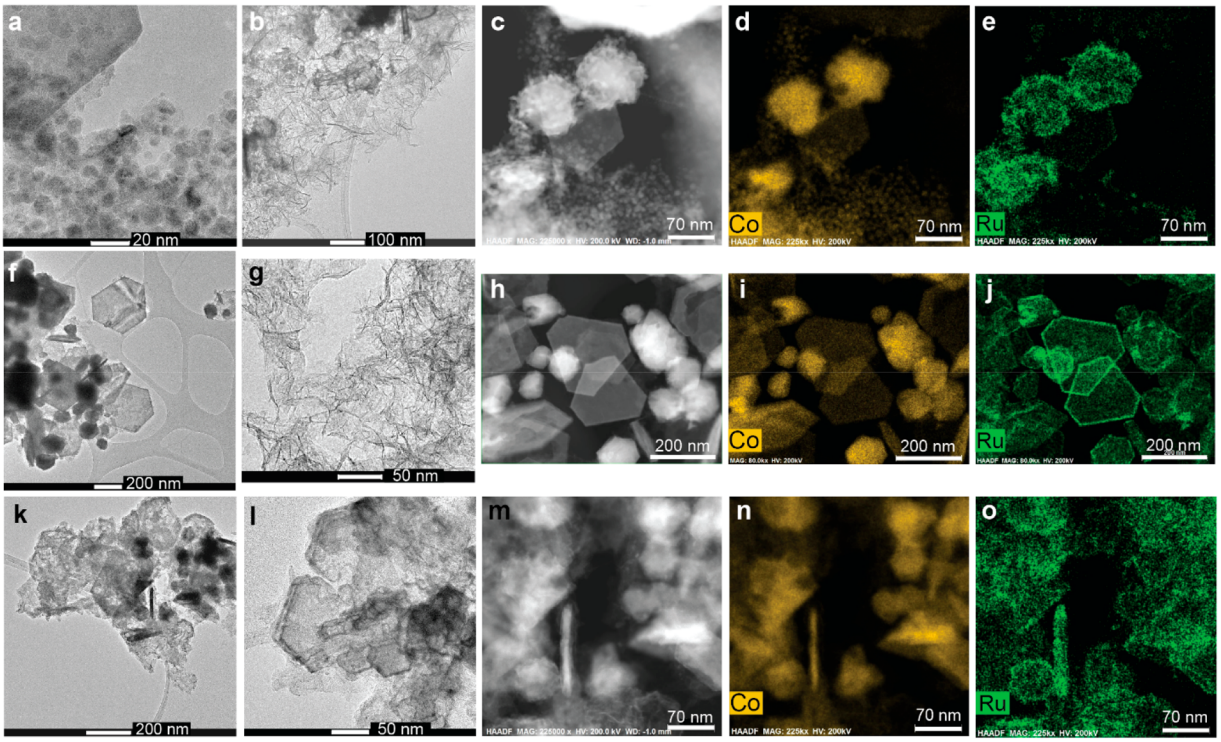

Figure 8. TEM and STEM images and EDS mapping of Ru@MFU-1 nanoparticles recovered from upgrading of 1-propanol (a–e), 1-butanol (f–j), and 1-pentanol (k–o).

mixture, however, gave rise to two distinct peaks, which were assigned to Ru^{II} and Ru^0 (Figure 7b). Similar reduction of part of the ruthenium content of **1** was observed when the ruthenium-incorporated MOF **1** was subjected to reduction with H_2 in isopropanol/benzene mixtures at 120 °C (Figure 7d). We conclude that a substantial fraction of the ruthenium content of **1** is reduced to the zerovalent state under the reaction conditions of alcohol upgrading, with H_2 presumed to be the reducing agent.

In the conversion of Ru@MFU-1 to the active catalyst, a fraction of the cobalt cations forming part of the secondary building unit (SBU) of the MOF support is incorporated into catalytically active RuCo alloy nanoparticles. Co 2p XPS analysis (Figure S20) revealed the presence of Co^0 alongside Co^{II}, but a quantitative analysis of Co^0 was complicated by the complex multiplet structure of Co^{II}.[71] To verify that reduction of a fraction of cobalt species occurs under the reaction conditions, we turned our attention to N 1s XPS of the bisdimethylprazolephenyl ligand present in MFU-1 (Figure S21). We observed a shift in the binding energy from 400.3 eV for the pyrazole linker bound to Co^{II} in the intact MOF structure to 398.8 eV after reduction of **1** with H_2. Catalyst **1** recovered from ethanol upgrading likewise displayed a decreased N 1s binding energy of 399.6 eV versus the pristine catalyst. We attribute the decrease in N 1s binding energy in both cases to reduction of a fraction of Co^{II} to a low-valent state, leading to decreased σ-donation from the pyrazolate ligand to the cobalt center.[72−74] The observation of a single N 1s XPS signal is inconsistent with the presence of notable amounts of pyrazole for which distinct sp^2 and sp^3 nitrogen signals separated by 1.3−1.8 eV would be expected, unlike the single peaks characteristic of metal-bound pyrazolates.[75,76] If reduction to form a free pyrazoline had occurred in the presence of H_2, one symmetrical signal around ∼400 eV would be expected, but such an assignment was considered unlikely due to the significantly lower binding energy of 398.8 eV observed upon reduction of **1** in the presence of H_2 (Figure S21b).[75] Interestingly, when the Guerbet reaction of 1-butanol promoted by 10 mol % NaOBu was carried out under an atmosphere of N_2, a TOF of 20 956 Ru^{-1} h^{-1} (Table S16) was observed for **1** (versus TOF = 17 416 Ru^{-1} h^{-1} for the equivalent reaction carried out under air (Table S4, entry 1)). The observed increase in catalytic activity upon exclusion of air is consistent with ruthenium and cobalt reduction during the formation of the active catalyst.

As expected, alloy nanoparticle formation in situ leads to a substantial decrease in the surface area of the recovered catalyst (181 ± 3 $m^2 \cdot g^{-1}$, Figure S22) versus pristine **1** (881 ± 19 $m^2 \cdot g^{-1}$, Figure 3) since a fraction of the cobalt is removed from the MOF's metal oxo clusters to yield RuCo. While the parts of the material that function as support for RuCo are presumed to largely retain the original MOF's connectivity, the lack of PXRD reflections attributable to MFU-1 indicate an absence of long-range order, so that a decrease in the accessible surface area would be expected.

EFFECT OF ALCOHOL SUBSTRATES ON NANOSTRUCTURE FORMATION

Importantly, for Guerbet reactions with MOF-derived Ru-alloy catalysts, the catalytically active species is formed in situ, and to maximize the space-time yield, reactions are performed neat. The alcohol, thus, simultaneously serves as the substrate and as the reaction medium for the formation of the catalytically active species. We compared TEM, scanning transmission electron microscopy (STEM) and energy dispersive X-ray spectroscopy (EDS) imaging data for catalyst **1** recovered from ethanol, 1-propanol, 1-butanol, and 1-pentanol upgrading reactions, respectively, to determine if the structural differences

https://doi.org/10.1021/acsami.1c09873
ACS Appl. Mater. Interfaces XXXX, XXX, XXX−XXX

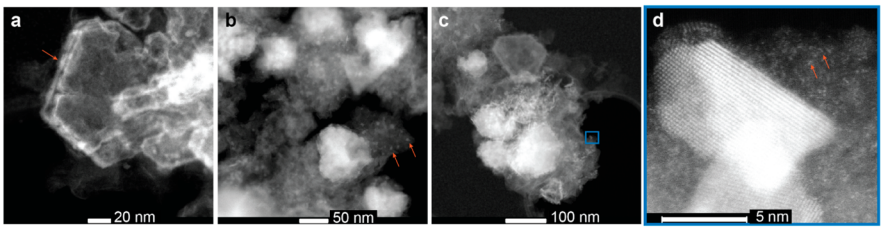

Figure 9. STEM images of Ru@MFU-1 nanoparticles recovered from upgrading of 1-pentanol (a, b) and 1-propanol (c, d) showing the presence of small ruthenium nanoparticles and isolated ruthenium atom on the support matrix.

exist between the nanoparticles formed in situ (Figure 8). We found that RuCo particles formed in ethanol not only were substantially larger (400 nm to 1 μm, Figure S23a−c) than those recovered from upgrading reactions of higher alcohols, but also appeared to be more effectively mixed with regard to Ru and Co. Efficient alloy formation was also observed in the previously reported ethanol upgrading reaction with Ru(nbd)-Cl_2@$Ni_8(OH)_4(OH_2)_2(tet)_6$ (tet = 2,6-bis(1*H*-pyrazol-4-yl)-pyrrolo[3,4-*f*]isoindole-1,3,5,7(2*H*,6*H*)-tetrone) where $Ru_{0.05}Ni_{0.95}$ alloy nanoparticles of relatively uniform distribution and 4.3 nm size were observed.[38] While only dense spherical particles were recovered from ethanol upgrading reactions, formation of the active catalyst in propanol, butanol, and pentanol additionally led to the formation of nanoplate morphology (Figure 8b, g, l). The nanoplates could be most clearly visualized in the case of butanol upgrading, where they are 200−300 nm in diameter (Figure 8f, h) but display only a thickness of a few atomic layers. The dense spherical particles observed in **1** recovered from 1-propanol, 1-butanol, and 1-pentanol upgrading were around 50−200 nm in size, and in the case of propanol, smaller 5−10 nm particles were additionally observed (Figure 8a, c). For alcohols other than ethanol, ruthenium is more accurately described as decorating the edges of cobalt-rich nanoparticles rather than as being incorporated into a homogeneous substitutional alloy (Figures 8d−e, i−j, n−o, S24, and S26). The clear morphological differences between the nanostructures formed in ethanol and those obtained with higher alcohol substrates are a possible source for the lower activity observed in ethanol upgrading versus the other alcohols. In addition to the enrichment of Ru on the edges of CoO_x nanostructures, small Ru nanoparticles (2−5 nm) and isolated Ru atoms were also found on the support matrix for both 1-propanol and 1-pentanol-derived **1** (Figures 9b, d and S25c, S28, and S29).

Enrichment of ruthenium nanoparticles on the edges of the support material is apparent from the darkened edges of the support observed in TEM (Figure 8l) and light edges found in STEM (Figure 9a) images. Elemental mapping (Figure S27) confirmed that the small nanoparticles on the support material were composed of ruthenium rather than cobalt. High-resolution STEM imaging also permitted detection of isolated ruthenium atoms dispersed over the support matrix in catalyst samples recovered from both 1-propanol upgrading (Figure 9d) and 1-pentanol upgrading (Figure S29). The ruthenium-doped cobalt MOF, which serves as a template for both the catalyst and its support material, contains cobalt in the form of metal oxo nodes (Co_4O) separated by organic linkers and ruthenium in the form of isolated molecules occupying the MOF pores. Upon partial decomposition of the MOF during the Guerbet reaction, a substantial fraction of cobalt agglomerates to large nanostructures, whereas ruthenium gives rise to small nanoparticles and isolated atoms on the support matrix, as well as forming a thin shell on cobalt oxide nanoparticles (Figures S24−S30). The formation of a catalyst with high ruthenium dispersion that is maintained at high temperature and in the presence of strong base may be attributable to spatial separation of the noble metal by organic linkers in the Ru(diene)Cl_2@MFU-1 precatalyst, which could be achieved by simple adsorption of a commercially available ruthenium precursor into the MOF pores.

CONCLUSION

We have shown that the selectivity and specificity of MOF-derived Guerbet catalysts can be tuned by the choice of MOF template: while RuNi nanoparticles derived from Ru@$Ni_8(OH)_4(OH_2)_2(tet)_6$ serve as selective catalysts for the synthesis of linear Guerbet product 1-butanol, RuCo nanostructures derived from **1** can efficiently and selectively furnish a suite of branched Guerbet products. High catalytic activity can be achieved in the presence of either a sodium alkoxide promoter or K_3PO_4, the use of which effectively eliminates a common Guerbet side reaction, which forms carboxylate salts. An XAS study of the precatalyst revealed that, in general, no substantial change in the ruthenium coordination sphere occurs upon introduction into the MOF. Use of $Ru_2Cl_4(CO)_6$ as the ruthenium precursor, however, leads to interactions between incorporated ruthenium compound and the MOF support discernible by IR. XPS analysis of **1** indicated that both Ru and Co are partially reduced under the reaction conditions of alcohol upgrading, and (S)TEM/EDS analysis revealed the formation of different nanostructures depending on whether ethanol or higher alcohols are employed as the reaction medium.

ASSOCIATED CONTENT

Supporting Information

The Supporting Information is available free of charge at https://pubs.acs.org/doi/10.1021/acsami.1c09873.

Detailed experimental procedure for alcohol upgrading; gas chromatograms; NMR quantification of potassium carboxylate formation; UV−vis and TEM data showing nanoparticle leaching in ethanol upgrading; data on reference reactions; XAS data for **1**; experimental procedure for the preparation of $Ru_2Cl_4(CO)_6$@MFU-1; PXRD, gas sorption, TGA, and IR data of $Ru_2Cl_4(CO)_6$@MFU-1; Co 2p and N 1s XPS data of **1**; and TEM, STEM, and EDS images of catalysts recovered from alcohol upgrading reactions (PDF)

https://doi.org/10.1021/acsami.1c09873
ACS Appl. Mater. Interfaces XXXX, XXX, XXX−XXX

AUTHOR INFORMATION

Corresponding Author

Mircea Dincă − *Department of Chemistry, Massachusetts Institute of Technology, Cambridge, Massachusetts 02139, United States;* orcid.org/0000-0002-1262-1264; Email: mdinca@mit.edu

Authors

Constanze N. Neumann − *Department of Chemistry, Massachusetts Institute of Technology, Cambridge, Massachusetts 02139, United States;* Present Address: Department of Heterogeneous Catalysis, Max-Planck-Institut für Kohlenforschung, Kaiser-Wilhelm-Platz 1, 45470 Mülheim, Germany

Michael T. Payne − *Department of Chemistry, Massachusetts Institute of Technology, Cambridge, Massachusetts 02139, United States*

Steven J. Rozeveld − *Core R&D, The Dow Chemical Company, Midland, Michigan 48674, United States*

Zhenwei Wu − *Davidson School of Chemical Engineering, Purdue University, West Lafayette, Indiana 47907, United States*

Guanghui Zhang − *Davidson School of Chemical Engineering, Purdue University, West Lafayette, Indiana 47907, United States*

Robert J. Comito − *Department of Chemistry, Massachusetts Institute of Technology, Cambridge, Massachusetts 02139, United States;* orcid.org/0000-0003-1298-2876

Jeffrey T. Miller − *Davidson School of Chemical Engineering, Purdue University, West Lafayette, Indiana 47907, United States;* orcid.org/0000-0002-6269-0620

Complete contact information is available at: https://pubs.acs.org/10.1021/acsami.1c09873

Notes

The authors declare the following competing financial interest(s): M.D. and C.N.N. are inventors on a patent application describing some of the results herein.

ACKNOWLEDGMENTS

This work was supported by Dow. We thank Dr. Robert W. Day for XPS data collection, Dr. Loredana Protesescu for collecting the TEM images in S13, and Dr. Ashley M. Wright for providing a sample of MFU-4*l*-(OH).[77]

REFERENCES

(1) Kohli, K.; Prajapati, R.; Sharma, B. K. Bio-Based Chemicals from Renewable Biomass for Integrated Biorefineries. *Energies* **2019**, *12* (2), 233.

(2) Palkovits, R.; Delidovich, I. Efficient Utilization of Renewable Feedstocks: the Role of Catalysis and Process Design. *Philos. Trans. R. Soc., A* **2018**, *376* (2110), 20170064.

(3) Gabriëls, D.; Hernández, W. Y.; Sels, B.; Van Der Voort, P.; Verberckmoes, A. Review of Catalytic Systems and Thermodynamics for the Guerbet Condensation Reaction and Challenges for Biomass Valorization. *Catal. Sci. Technol.* **2015**, *5* (8), 3876−3902.

(4) Ndaba, B.; Adeleke, R.; Makofane, R.; Daramola, M. O.; Moshokoa, M., Butanol as a Drop-In Fuel: A Perspective on Production Methods and Current Status. In *Valorization of Biomass to Value-Added Commodities: Current Trends, Challenges, and Future Prospects*; Daramola, M. O., Ayeni, A. O., Eds.; Springer International Publishing: Cham, 2020; pp 371−398.

(5) Nanda, S.; Rana, R.; Vo, D.-V. N.; Sarangi, P. K.; Nguyen, T. D.; Dalai, A. K.; Kozinski, J. A., A Spotlight on Butanol and Propanol as Next-Generation Synthetic Fuels. In *Biorefinery of Alternative Resources: Targeting Green Fuels and Platform Chemicals*; Nanda, S., N. Vo, D.-V., Sarangi, P. K., Eds.; Springer: Singapore, 2020; pp 105−126.

(6) Bond-Watts, B. B.; Bellerose, R. J.; Chang, M. C. Y. Enzyme Mechanism as a Kinetic Control Element for Designing Synthetic Biofuel Pathways. *Nat. Chem. Biol.* **2011**, *7* (4), 222−227.

(7) Millat, T.; Winzer, K. Mathematical Modelling of Clostridial Acetone-Butanol-Ethanol Fermentation. *Appl. Microbiol. Biotechnol.* **2017**, *101* (6), 2251−2271.

(8) Baral, N. R.; Shah, A. Techno-Economic Analysis of Cellulosic Butanol Production from Corn Stover through Acetone-Butanol-Ethanol Fermentation. *Energy Fuels* **2016**, *30* (7), 5779−5790.

(9) Liu, X.; Yu, X. Enhancement of Butanol Production: From Biocatalysis to Bioelectrocatalysis. *ACS Energy Lett.* **2020**, *5* (3), 867−878.

(10) Marcu, I.-C.; Tanchoux, N.; Fajula, F.; Tichit, D. Catalytic Conversion of Ethanol into Butanol over M-Mg-Al Mixed Oxide Catalysts (M = Pd, Ag, Mn, Fe, Cu, Sm, Yb) Obtained from LDH Precursors. *Catal. Lett.* **2013**, *143* (1), 23−30.

(11) Pang, J.; Zheng, M.; He, L.; Li, L.; Pan, X.; Wang, A.; Wang, X.; Zhang, T. Upgrading Ethanol to n-Butanol over Highly Dispersed Ni-MgAlO Catalysts. *J. Catal.* **2016**, *344*, 184−193.

(12) Wu, X.; Fang, G.; Liang, Z.; Leng, W.; Xu, K.; Jiang, D.; Ni, J.; Li, X. Catalytic Upgrading of Ethanol to n-Butanol over M-CeO2/AC (M = Cu, Fe, Co, Ni and Pd) Catalysts. *Catal. Commun.* **2017**, *100*, 15−18.

(13) Wu, X.; Fang, G.; Tong, Y.; Jiang, D.; Liang, Z.; Leng, W.; Liu, L.; Tu, P.; Wang, H.; Ni, J.; Li, X. Catalytic Upgrading of Ethanol to n-Butanol: Progress in Catalyst Development. *ChemSusChem* **2018**, *11* (1), 71−85.

(14) Vlasenko, N. V.; Kyriienko, P. I.; Valihura, K. V.; Kosmambetova, G. R.; Soloviev, S. O.; Strizhak, P. E. Yttria-Stabilized Zirconia as a High-Performance Catalyst for Ethanol to n-Butanol Guerbet Coupling. *ACS Omega* **2019**, *4* (25), 21469−21476.

(15) Wang, D.; Liu, Z.; Liu, Q. Efficient Conversion of Ethanol to 1-Butanol and C5-C9 Alcohols over Calcium Carbide. *RSC Adv.* **2019**, *9* (33), 18941−18948.

(16) Wang, D.; Liu, Z.; Liu, Q. Synthesis of 1-Butanol from Ethanol over Calcium Ethoxide: Experimental and Density Functional Theory Simulation. *J. Phys. Chem. C* **2019**, *123* (37), 22932−22940.

(17) Larina, O. V.; Valihura, K. V.; Kyriienko, P. I.; Vlasenko, N. V.; Balakin, D. Y.; Khalakhan, I.; Čendak, T.; Soloviev, S. O.; Orlyk, S. M. Successive Vapour Phase Guerbet Condensation of Ethanol and 1-Butanol over Mg-Al Oxide Catalysts in a Flow Reactor. *Appl. Catal., A* **2019**, *588*, 117265.

(18) Wang, H.; Miao, G.; Kong, L.; Luo, H.; Zhang, Y.; Zhao, X.; Li, S.; Sun, Y. Efficient One-Pot Valorization of Ethanol to 1-Butanol over an Earth-Abundant Ni-MgO Catalyst under Mild Conditions. *Sustain. Energy Fuels* **2020**, *4* (4), 1612−1615.

(19) Pang, J.; Zheng, M.; Wang, Z.; Liu, S.; Li, X.; Li, X.; Wang, J.; Zhang, T. Catalytic Upgrading of Ethanol to Butanol over a Binary Catalytic System of FeNiOx and LiOH. *Chin. J. Catal.* **2020**, *41* (4), 672−678.

(20) Zhang, J.; Shi, K.; An, Z.; Zhu, Y.; Shu, X.; Song, H.; Xiang, X.; He, J. Acid-Base Promoted Dehydrogenation Coupling of Ethanol on Supported Ag Particles. *Ind. Eng. Chem. Res.* **2020**, *59* (8), 3342−3350.

(21) Zhang, Q.; Liu, W.; Chen, B.; Qiu, S.; Wang, T. Upgrading of Aqueous Ethanol to Fuel Grade Higher Alcohols over Dandelion-like Ni-Sn Catalyst. *Energy Convers. Manage.* **2020**, *216*, 112914.

(22) Zhu, Q.; Yin, L.; Ji, K.; Li, C.; Wang, B.; Tan, T. Effect of Catalyst Structure and Acid-Base Property on the Multiproduct Upgrade of Ethanol and Acetaldehyde to C4 (Butadiene and Butanol) over the Y-SiO2 Catalysts. *ACS Sustainable Chem. Eng.* **2020**, *8* (3), 1555−1565.

(23) Wang, Z.; Pang, J.; Song, L.; Li, X.; Yuan, Q.; Li, X.; Liu, S.; Zheng, M. Conversion of Ethanol to n-Butanol over NiCeO2 Based

Catalysts: Effects of Metal Dispersion and NiCe Interactions. *Ind. Eng. Chem. Res.* **2020**, *59* (51), 22057−22067.
(24) Nezam, I.; Zak, J.; Miller, D. J. Condensed-Phase Ethanol Conversion to Higher Alcohols over Bimetallic Catalysts. *Ind. Eng. Chem. Res.* **2020**, *59* (31), 13906−13915.
(25) Larina, O. V.; Valihura, K. V.; Kyriienko, P. I.; Vlasenko, N. V.; Balakin, D. Y.; Khalakhan, I.; Veltruská, K.; Čendak, T.; Soloviev, S. O.; Orlyk, S. M. Catalytic Performance of Ternary Mg-Al-Ce Oxides for Ethanol Conversion into 1-Butanol in a Flow Reactor. *J. Fuel Chem. Technol.* **2021**, *49* (3), 347−358.
(26) Dowson, G. R. M.; Haddow, M. F.; Lee, J.; Wingad, R. L.; Wass, D. F. Catalytic Conversion of Ethanol into an Advanced Biofuel: Unprecedented Selectivity for n-Butanol. *Angew. Chem., Int. Ed.* **2013**, *52* (34), 9005−9008.
(27) Aitchison, H.; Wingad, R. L.; Wass, D. F. Homogeneous Ethanol to Butanol Catalysis—Guerbet Renewed. *ACS Catal.* **2016**, *6* (10), 7125−7132.
(28) Chakraborty, S.; Piszel, P. E.; Hayes, C. E.; Baker, R. T.; Jones, W. D. Highly Selective Formation of n-Butanol from Ethanol through the Guerbet Process: A Tandem Catalytic Approach. *J. Am. Chem. Soc.* **2015**, *137* (45), 14264−14267.
(29) Tseng, K.-N. T.; Lin, S.; Kampf, J. W.; Szymczak, N. K. Upgrading Ethanol to 1-Butanol with a Homogeneous Air-Stable Ruthenium Catalyst. *Chem. Commun.* **2016**, *52* (14), 2901−2904.
(30) Xie, Y.; Ben-David, Y.; Shimon, L. J. W.; Milstein, D. Highly Efficient Process for Production of Biofuel from Ethanol Catalyzed by Ruthenium Pincer Complexes. *J. Am. Chem. Soc.* **2016**, *138* (29), 9077−9080.
(31) Fu, S.; Shao, Z.; Wang, Y.; Liu, Q. Manganese-Catalyzed Upgrading of Ethanol into 1-Butanol. *J. Am. Chem. Soc.* **2017**, *139* (34), 11941−11948.
(32) Kulkarni, N. V.; Brennessel, W. W.; Jones, W. D. Catalytic Upgrading of Ethanol to n-Butanol via Manganese-Mediated Guerbet Reaction. *ACS Catal.* **2018**, *8* (2), 997−1002.
(33) Mazzoni, R.; Cesari, C.; Zanotti, V.; Lucarelli, C.; Tabanelli, T.; Puzzo, F.; Passarini, F.; Neri, E.; Marani, G.; Prati, R.; Viganò, F.; Conversano, A.; Cavani, F. Catalytic Biorefining of Ethanol from Wine Waste to Butanol and Higher Alcohols: Modeling the Life Cycle Assessment and Process Design. *ACS Sustainable Chem. Eng.* **2019**, *7* (1), 224−237.
(34) DiBenedetto, T. A.; Jones, W. D. Upgrading of Ethanol to n-Butanol via a Ruthenium Catalyst in Aqueous Solution. *Organometallics* **2021**, *40* (12), 1884−1888.
(35) Burk, P. L.; Pruett, R. L.; Campo, K. S. The Rhodium-Promoted Guerbet Reaction: Part I. Higher Alcohols from Lower Alcohols. *J. Mol. Catal.* **1985**, *33* (1), 1−14.
(36) Gregorio, G.; Pregaglia, G. F.; Ugo, R. Condensation of Alcohols Catalysed by Tertiary Phosphine Transition Metal Complexes. *J. Organomet. Chem.* **1972**, *37* (2), 385−387.
(37) Carlini, C.; Macinai, A.; Marchionna, M.; Noviello, M.; Galletti, A. M. R.; Sbrana, G. Selective Synthesis of Isobutanol by Means of the Guerbet Reaction: Part 3: Methanol/n-Propanol Condensation by Using Bifunctional Catalytic Systems Based on Nickel, Rhodium and Ruthenium Species with Basic Components. *J. Mol. Catal. A: Chem.* **2003**, *206* (1), 409−418.
(38) Neumann, C. N.; Rozeveld, S. J.; Yu, M.; Rieth, A. J.; Dincă, M. Metal-Organic Framework-Derived Guerbet Catalyst Effectively Differentiates between Ethanol and Butanol. *J. Am. Chem. Soc.* **2019**, *141* (44), 17477−17481.
(39) Neumann, C. N.; Rozeveld, S. J.; Dincă, M. MOF-Derived RuCo Catalyzes the Formation of a Plasticizer Alcohol from Renewable Precursors. *ACS Catal.* **2021**, *11*, 8521−8526.
(40) O'Lenick, A. J., Jr. Guerbet Chemistry. *J. Surfactants Deterg.* **2001**, *4* (3), 311−315.
(41) Wang, K.; Zhang, L.; Tang, W.; Sun, H.; Xue, D.; Lei, M.; Xiao, J.; Wang, C. Asymmetric Guerbet Reaction to Access Chiral Alcohols. *Angew. Chem., Int. Ed.* **2020**, *59* (28), 11408−11415.
(42) Guerbet, M. C. Action de l'Alcool Amylique de Fermentation sur son Dèrivé Sodé. *R. Hebd. Séances Acad. Sci.* **1899**, *128*, 511−513.
(43) Markownikoff, W.; Zuboff, P. Über die Condensation Höherer Alkohole: Tricaprylalkohol. *Ber. Dtsch. Chem. Ges.* **1901**, *34* (3), 3246−3249.
(44) Miller, R.; Bennett, G. Producing 2-Ethylhexanol by the Guerbet Reaction. *Ind. Eng. Chem.* **1961**, *53* (1), 33−36.
(45) Carlini, C.; Macinai, A.; Raspolli Galletti, A. M.; Sbrana, G. Selective Synthesis of 2-Ethyl-1-Hexanol from n-Butanol through the Guerbet Reaction by Using Bifunctional Catalysts Based on Copper or Palladium Precursors and Sodium Butoxide. *J. Mol. Catal. A: Chem.* **2004**, *212* (1), 65−70.
(46) Xu, G.; Lammens, T.; Liu, Q.; Wang, X.; Dong, L.; Caiazzo, A.; Ashraf, N.; Guan, J.; Mu, X. Direct Self-Condensation of Bio-Alcohols in the Aqueous Phase. *Green Chem.* **2014**, *16* (8), 3971−3977.
(47) Liu, D.; Chen, X.; Xu, G.; Guan, J.; Cao, Q.; Dong, B.; Qi, Y.; Li, C.; Mu, X. Iridium Nanoparticles Supported on Hierarchical Porous N-Doped Carbon: an Efficient Water-Tolerant Catalyst for Bio-Alcohol Condensation in Water. *Sci. Rep.* **2016**, *6*, 21365.
(48) Panchenko, V. N.; Paukshtis, E. A.; Murzin, D. Y.; Simakova, I. L. Solid Base Assisted n-Pentanol Coupling over VIII Group Metals: Elucidation of the Guerbet Reaction Mechanism by DRIFTS. *Ind. Eng. Chem. Res.* **2017**, *56* (45), 13310−13321.
(49) Wang, J.; Yang, W.; Wu, C.; Gong, Y.; Zhang, J.; Shen, C. Upgrading n-Butanol to Branched Alcohols over Ni/CaxMgyO. *ACS Sustainable Chem. Eng.* **2020**, *8* (45), 16960−16967.
(50) Han, X.; An, H.; Zhao, X.; Wang, Y. Influence of Acid-Base Properties on the Catalytic Performance of Ni/Hydroxyapatite in n-Butanol Guerbet Condensation. *Catal. Commun.* **2020**, *146*, 106130.
(51) Xu, Z.; Yan, P.; Liang, C.; Jia, S.; Liu, X.; Zhang, Z. C. Electronic and Steric Factors for Enhanced Selective Synthesis of 2-Ethyl-1-hexanol in the Ir-Complex-Catalyzed Guerbet Reaction of 1-Butanol. *Chin. J. Catal.* **2021**, *42* (9), 1586−1592.
(52) Tonigold, M.; Lu, Y.; Bredenkötter, B.; Rieger, B.; Bahnmüller, S.; Hitzbleck, J.; Langstein, G.; Volkmer, D. Heterogeneous Catalytic Oxidation by MFU-1: A Cobalt(II)-Containing Metal-Organic Framework. *Angew. Chem., Int. Ed.* **2009**, *48* (41), 7546−7550.
(53) Tonigold, M.; Lu, Y.; Mavrandonakis, A.; Puls, A.; Staudt, R.; Möllmer, J.; Sauer, J.; Volkmer, D. Pyrazolate-Based Cobalt(II)-Containing Metal-Organic Frameworks in Heterogeneous Catalytic Oxidation Reactions: Elucidating the Role of Entatic States for Biomimetic Oxidation Processes. *Chem. - Eur. J.* **2011**, *17* (31), 8671−8695.
(54) Cherepakhin, V.; Williams, T. J. Iridium Catalysts for Acceptorless Dehydrogenation of Alcohols to Carboxylic Acids: Scope and Mechanism. *ACS Catal.* **2018**, *8* (5), 3754−3763.
(55) King, A. M.; Sparkes, H. A.; Wingad, R. L.; Wass, D. F. Manganese Diphosphine and Phosphinoamine Complexes Are Effective Catalysts for the Production of Biofuel Alcohols via the Guerbet Reaction. *Organometallics* **2020**, *39* (21), 3873−3878.
(56) Wethman, R.; Derosa, J.; Tran, V. T.; Kang, T.; Apolinar, O.; Abraham, A.; Kleinmans, R.; Wisniewski, S. R.; Coombs, J. R.; Engle, K. M. An Under-Appreciated Source of Reproducibility Issues in Cross-Coupling: Solid-State Decomposition of Primary Sodium Alkoxides in Air. *ACS Catal.* **2021**, *11*, 502−508.
(57) Creighton, J. A.; Eadon, D. G. Ultraviolet-Visible Absorption Spectra of the Colloidal Metallic Elements. *J. Chem. Soc., Faraday Trans.* **1991**, *87* (24), 3881−3891.
(58) Zawadzki, M.; Okal, J. Synthesis and Structure Characterization of Ru Nanoparticles Stabilized by PVP or γ-Al2O3. *Mater. Res. Bull.* **2008**, *43* (11), 3111−3121.
(59) Han, X.; Li, S.; An, H.; Zhao, X.; Wang, Y. Improvement of n-butanol Guerbet condensation: a reaction integration of n-butanol Guerbet condensation and 1,1-dibutoxybutane hydrolysis. *React. Chem. Eng.* **2021**, DOI: 10.1039/D1RE00206F.
(60) Tonigold, M.; Lu, Y.; Mavrandonakis, A.; Puls, A.; Staudt, R.; Mollmer, J.; Sauer, J.; Volkmer, D. Pyrazolate-based cobalt(II)-containing metal-organic frameworks in heterogeneous catalytic oxidation reactions: elucidating the role of entatic states for biomimetic oxidation processes. *Chem. - Eur. J.* **2011**, *17* (31), 8671−95.

https://doi.org/10.1021/acsami.1c09873
ACS Appl. Mater. Interfaces XXXX, XXX, XXX−XXX

(61) Vollmer, C.; Schröder, M.; Thomann, Y.; Thomann, R.; Janiak, C. Turning Teflon-Coated Magnetic Stirring Bars to Catalyst Systems with Metal Nanoparticle Trace Deposits - A Caveat and a Chance. *Appl. Catal., A* **2012**, *425−426*, 178−183.
(62) Pentsak, E. O.; Eremin, D. B.; Gordeev, E. G.; Ananikov, V. P. Phantom Reactivity in Organic and Catalytic Reactions as a Consequence of Microscale Destruction and Contamination-Trapping Effects of Magnetic Stir Bars. *ACS Catal.* **2019**, *9* (4), 3070−3081.
(63) Gitnes, R. M.; Wang, M.; Bao, Y.; Scheuermann, M. L. In Situ Generation of Catalytically Relevant Nanoparticles from a Molecular Pincer Iridium Precatalyst during Polyol Deoxygenation. *ACS Catal.* **2021**, *11*, 495−501.
(64) Benedetti, E.; Braca, G.; Sbrana, G.; Salvetti, F.; Grassi, B. Infrared Spectra and Reactivity of Di-μ-Halobis-(halotricarbonylruthenium). *J. Organomet. Chem.* **1972**, *37* (2), 361−373.
(65) Balducci, G.; Iengo, E.; Demitri, N.; Alessio, E. New Insight into a Deceptively Simple Reaction: The Coordination of bpy to RuII-Carbonyl Precursors - The Central Role of the fac-$[Ru(bpy)Cl(CO)_3]^+$ Intermediate and the Chloride Rebound Mechanism. *Eur. J. Inorg. Chem.* **2015**, *2015* (26), 4296−4311.
(66) Jakonen, M.; Hirva, P.; Nivajärvi, T.; Kallinen, M.; Haukka, M. Surface-Assisted Synthesis and Behavior of Dimetallic Mixed-Metal Complexes $[M_2Cl_2(\mu\text{-}Cl)_4(CO)6M'(L)_2]$ (M = Ru, Os; M′ = Fe, Co; L = CH_3CH_2OH, H_2O). *Eur. J. Inorg. Chem.* **2007**, *2007* (22), 3497−3508.
(67) Moreno, M. A.; Haukka, M.; Kallinen, M.; Pakkanen, T. A. Reactions of $[Ru(CO)_3Cl_2]_2$ with Aromatic Nitrogen Donor Ligands in Alcoholic Media. *Appl. Organomet. Chem.* **2006**, *20* (1), 51−69.
(68) Wang, P.; Liu, H.; Zhao, Q.; Chen, Y.; Liu, B.; Zhang, B.; Zheng, Q. Syntheses and Evaluation of Drug-Like Properties of CO-Releasing Molecules Containing Ruthenium and Group 6 Metal. *Eur. J. Med. Chem.* **2014**, *74*, 199−215.
(69) Wang, C.-H.; Gao, W.-Y.; Ma, Q.; Powers, D. C. Templating Metastable Pd2 Carboxylate Aggregates. *Chem. Sci.* **2019**, *10* (6), 1823−1830.
(70) He, T.; Kong, X.-J.; Zhou, J.; Zhao, C.; Wang, K.; Wu, X.-Q.; Lv, X.-L.; Si, G.-R.; Li, J.-R.; Nie, Z.-R. A Practice of Reticular Chemistry: Construction of a Robust Mesoporous Palladium Metal-Organic Framework via Metal Metathesis. *J. Am. Chem. Soc.* **2021**, *143* (26), 9901−9911.
(71) Biesinger, M. C.; Lau, L. W. M.; Gerson, A. R.; Smart, R. S. C. Resolving Surface Chemical States in XPS Analysis of First Row Transition Metals, Oxides and Hydroxides: Sc, Ti, V, Cu and Zn. *Appl. Surf. Sci.* **2010**, *257* (3), 887−898.
(72) Skomski, D.; Tempas, C. D.; Cook, B. J.; Polezhaev, A. V.; Smith, K. A.; Caulton, K. G.; Tait, S. L. Two- and Three-Electron Oxidation of Single-Site Vanadium Centers at Surfaces by Ligand Design. *J. Am. Chem. Soc.* **2015**, *137* (24), 7898−902.
(73) Brown, D. G.; Weser, U. XPS Spectra of Copper and Nickel Biuret Complexes — Observations of Intense Satellite Structure in the 2P Spectrum of a Copper(III) System. *Z. Naturforsch., B: J. Chem. Sci.* **1979**, *34* (7), 989−994.
(74) Lionetti, D.; Day, V. W.; Blakemore, J. D. Noncovalent Immobilization and Surface Characterization of Lanthanide Complexes on Carbon Electrodes. *Dalton Trans.* **2017**, *46* (35), 11779−11789.
(75) Katrib, A.; El-Rayyes, N. R.; Al-Kharafi, F. M. N 1s Orbital Binding Energies of Some Pyrazole Pyrazoline Compounds by XPS. *J. Electron Spectrosc. Relat. Phenom.* **1983**, *31* (3), 317−321.
(76) Jhuang, J.-Y.; Lee, S.-H.; Chen, S.-W.; Chen, Y.-H.; Chen, Y.-J.; Lin, J.-L.; Wang, C.-H.; Yang, Y.-W. Adsorption and Reaction Pathways of 1H-Pyrazole on Cu(100) and O/Cu(100). *J. Phys. Chem. C* **2018**, *122* (11), 6195−6208.
(77) Wright, A. M.; Wu, Z.; Zhang, G.; Mancuso, J. L.; Comito, R. J.; Day, R. W.; Hendon, C. H.; Miller, J. T.; Dincă, M. A Structural Mimic of Carbonic Anhydrase in a Metal-Organic Framework. *Chem.* **2018**, *4* (12), 2894−2901.

https://doi.org/10.1021/acsami.1c09873
ACS Appl. Mater. Interfaces XXXX, XXX, XXX−XXX